*crystals*

*Article*

# Phase Relations of $Ni_2In$-Type and $CaC_2$-Type Structures Relative to $Fe_2P$-Type Structure of Titania at High Pressure: A Comparative Study

**Khaldoun Tarawneh * and Yahya Al-Khatatbeh**

Department of Basic Sciences, Princess Sumaya University for Technology, Amman 11941, Jordan
* Correspondence: khaldoun@psut.edu.jo

**Abstract:** Density functional theory (DFT) based on *first-principles* calculations was used to study the high-pressure phase stability of various phases of titanium dioxide ($TiO_2$) at extreme pressures. We explored the phase relations among the following phases: the experimentally identified nine-fold hexagonal $Fe_2P$-type phase, the previously predicted ten-fold tetragonal $CaC_2$-type phase of $TiO_2$, and the recently proposed eleven-fold hexagonal $Ni_2In$-type phase of the similar dioxides zirconia ($ZrO_2$) and hafnia ($HfO_2$). Our calculations, using the generalized gradient approximation (GGA), predicted the $Fe_2P \rightarrow Ni_2In$ transition to occur at 564 GPa and $Fe_2P \rightarrow CaC_2$ at 664 GPa. These transitions were deeply investigated with reference to the volume reduction, coordination number decrease, and band gap narrowing to better determine the favorable post-$Fe_2P$ phase. Furthermore, it was found that both transitions are mostly driven by the volume reduction across transitions in comparison with the small contribution of the electronic energy gain. Additionally, our computed Birch–Murnaghan equation of state for the three phases reveals that $CaC_2$ is the densest phase, while $Ni_2In$ is the most compressible phase.

**Keywords:** phase transitions; enthalpy difference components; equation of state; first principles; phase relations; band gap

check for updates

**Citation:** Tarawneh, K.; Al-Khatatbeh, Y. Phase Relations of $Ni_2In$-Type and $CaC_2$-Type Structures Relative to $Fe_2P$-Type Structure of Titania at High Pressure: A Comparative Study. *Crystals* **2023**, *13*, 9. https://doi.org/10.3390/cryst13010009

Academic Editors: Daniel Errandonea and Enrico Bandiello

Received: 27 November 2022
Revised: 17 December 2022
Accepted: 18 December 2022
Published: 21 December 2022



## 1. Introduction

The nature of bonding in titania ($TiO_2$) has attracted great interest over the last few decades due to its interesting industrial applications such as photocatalysts, energy generation and storage, environmental protection, and many more [1,2]. One of the important and promising research directions in studying this dioxide is investigating the high-pressure behavior of $TiO_2$ polymorphs, both experimentally and theoretically, due to their interesting properties [3–39]. However, much attention, using measurements and calculations, has been given to exploring the high-pressure phase stability of $TiO_2$ phases and the transition pressures between different phases and their equation of state parameters as well as to searching for new possible phases (e.g., [3,8,11,15,18,19,21,22,29,31–33,37]). Over the past decades, density functional theory has become the workhorse theory for the identification of the pressure-driven phase transitions [40,41].

As mentioned above, titania can be found in many structural forms with increasing pressure. In this regard, the well-known transition sequence that is experimentally observed and theoretically predicted is as follows: Orthorhombic OI $\rightarrow$ orthorhombic cotunnite OII $\rightarrow$ $Fe_2P$-type [3,15,29,31]. Thus, the hexagonal $Fe_2P$-type structure (Figure 1a) is the highest-pressure phase experimentally observed for $TiO_2$ which has been found to be stable at (210 GPa, 4000 K) using diamond-anvil experiments [31]. Recently, the tetragonal $CaC_2$-type structure (Figure 1c) has been theoretically predicted as a post-$Fe_2P$ phase of titanium dioxide at pressures beyond 647–689 GPa [33,36]. Additionally, recent density functional theory (DFT) calculations have predicted the hexagonal $Ni_2In$-type structure

(Figure 1b) to be the post-$Fe_2P$ phase in the similar dioxides $ZrO_2$ and $HfO_2$ at pressures that exceed 300 GPa [42–44].

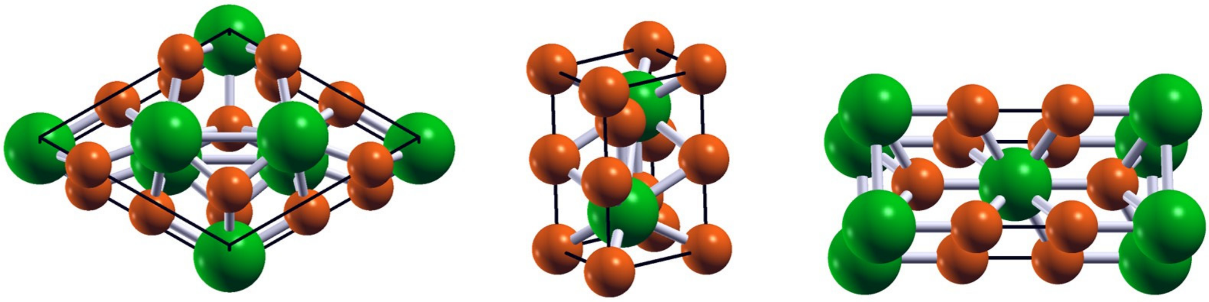

**(a)** $Fe_2P$-type structure **(b)** $Ni_2In$-type structure **(c)** $CaC_2$-type structure

**Figure 1.** Crystal structures of $TiO_2$ phases (generated using XCrySDen software [45]). The green spheres represent the titanium atom, while the alloy orange spheres represent the oxygen atom. (**a**) $Fe_2P$-type: crystal structure: hexagonal, space group: $P\overline{6}2m$, coordination number: 9, lattice parameters: $a = b = 5.3274$ Å and $c = 3.1234$ Å, atomic coordinates: Ti1 (1/3, 2/3, 1/2), Ti2 (0, 0, 0), O1 (0.262, 0, 1/2), O2 (0.601, 0, 0). (**b**) $Ni_2In$-type: crystal structure: hexagonal, space group: $P6_3/mmc$, coordination number: 11, lattice parameters: $a = b = 3.2632$ Å and $c = 6.0335$ Å, atomic coordinates: Ti (1/3, 2/3, 1/4), O1 (0, 0, 0), O2 (1/3, 2/3, 3/4). (**c**) $CaC_2$-type: crystal structure: tetragonal, space group: $I4/mmm$, coordination number: 10, lattice parameters: $a = b = 2.7407$ Å and $c = 6.7179$ Å, atomic coordinates: Ti (1/2, −1/2, 0), O (1, −1, 0.152).

However, it is important to note that the three dioxides ($TiO_2$, $ZrO_2$, and $HfO_2$) share obvious similarities, especially in their high-pressure behavior (e.g., see Ref. [26] and references therein). In this regard, the overlapping high-pressure phase transition sequence, experimentally observed and theoretically confirmed in the three dioxides is as follows: Monoclinic baddeleyite MI $\rightarrow$ OI $\rightarrow$ OII $\rightarrow$ $Fe_2P$ [3,15,26,29,31,46–50].

The obvious and close similarities of the high-pressure behavior of titania, zirconia, and hafnia have motivated us to test the stability of $Fe_2P$-$TiO_2$ with respect to $CaC_2$ and $Ni_2In$ phases. In detail, until recently, the theoretical work performed on $TiO_2$ predicted the $Fe_2P \rightarrow CaC_2$ transition [33,36], while the $Fe_2P \rightarrow Ni_2In$ transition was predicted in $ZrO_2$ and $HfO_2$ [42–44]. Therefore, to better understand the upper part of the phase transition sequence in $TiO_2$, we have performed DFT calculations to investigate the phase relations among $Fe_2P$, $CaC_2$, and $Ni_2In$ phases at megabar pressures. Consequently, the long-range target of this study is to draw the similarities and differences between $TiO_2$ and other similar transition-metal dioxides in terms of predicting the ultrahigh-pressure phase transition sequence, which will hopefully lead to a better understanding of the high-pressure behavior of such dioxides.

## 2. Computational Details

In order to investigate the phase stability and the equations of state (EOSs) of all tested phases of $TiO_2$, we used static *first-principles* computations performed within the framework of density functional theory (DFT) [51]. The projector-augmented wave (PAW) formalism [52,53] was used to treat the interactions between the titanium (Ti) and oxygen (O) atoms with the valence configuration of $3s^2 3p^6 3d^2 4s^2$ for Ti and $2s^2 2p^4$ for O. Following previous theoretical high-pressure studies carried out on $TiO_2$ and similar dioxides [29,43,44,46–48], the electronic exchange and correlation effects were treated within the GGA [54]. We performed our calculations using the Quantum ESPRESSO package [55] with an energy cutoff of 80 Ry and $\Gamma$-centered $k$-point meshes [56]. Our calculations yielded sufficient convergence to better than $10^{-5}$ Ry in the total energies for both phases, and pressures were converged to better than 0.1 GPa. The Brillouin zone integration was performed using the following $k$-point meshes for the $ZrO_2$ phases: $8 \times 8 \times 12$ for $Fe_2P$,

$12 \times 12 \times 8$ for $CaC_2$, and $20 \times 20 \times 16$ for $Ni_2In$. For a fixed volume, all internal degrees of freedom and unit-cell parameters of the structure were optimized simultaneously during the geometry optimizations. The ground-state energy for each phase was determined for 13–16 volumes, and the EOS parameters for each phase were obtained by fitting the total energy as a function of volume to a second-order Birch–Murnaghan equation of state (BM-EOS) [57] (Table 1). Phonon dispersion calculations have not been performed and will be the scope of future studies.

**Table 1.** Calculated equations of state for the $Fe_2P$, $Ni_2In$, and $CaC_2$ phases of $TiO_2$. Our EOS is determined from GGA calculations using the second-order BM-EOS [57]. For comparison, we list other calculated EOSs for $TiO_2$ and the similar dioxides $ZrO_2$ and $HfO_2$. 1σ uncertainties are given in parentheses.

| Phase | Equation of State | | | Reference |
|---|---|---|---|---|
| | $V_0$ (Å$^3$) | $K_0$ (GPa) | $K_0'$ | |
| $Fe_2P$-$TiO_2$ | 25.7 | 272.1 | 4 | [31] |
| | 25.53 | 287 | 4.1 | [32] |
| | 25.59 (0.03) | 284 (2) | 4 (fixed) | This work |
| $Fe_2P$-$ZrO_2$ | 30.17 | 248 | 3.76 | [42] |
| | 30.94 (0.03) | 272 (2) | 4 (fixed) | [44] |
| | 30.34 | 272 | 4 (fixed) | [48] |
| $Fe_2P$-$HfO_2$ | 29.73 (0.02) | 282 (2) | 4 (fixed) | [43] |
| | 29.69 (0.03) | 288 (2) | 4 (fixed) | [48] |
| | 29.8 | 284 | 4.2 | [50] |
| $Ni_2In$-$TiO_2$ | 27.82 (0.19) | 173 (6) | 4 (fixed) | This work |
| $Ni_2In$-$ZrO_2$ | 29.21 | 239 | 3.86 | [42] |
| | 31.81 (0.13) | 200 (5) | 4 (fixed) | [44] |
| $Ni_2In$-$HfO_2$ | 30.49 (0.14) | 213 (6) | 4 (fixed) | [43] |
| $CaC_2$-$TiO_2$ | 25.23 (0.04) | 264 (3) | 4 (fixed) | This work |

## 3. Results and Discussion

### *3.1. Phase Stability and Equation of State*

We computed our EOS parameters for each phase by fitting the energy-volume ($E$-$V$) data to the following second-order BM-EOS [57] for which the first pressure derivative of the bulk modulus at zero pressure ($K_0'$) was fixed to 4 and the zero-pressure volume ($V_0$) and the zero-pressure bulk modulus ($K_0$) were used as fitting parameters. The determination of the EOS for the three phases allowed us to investigate their compressibilities and phase stability at high pressure as well as the volume change across different transitions.

The EOS parameters for all phases are summarized in Table 1 along with results from previous calculations [31,32]. We note that our calculated EOS for the $Fe_2P$ phase agrees well with previous studies [31,32]. On the other hand, the EOS of either $Ni_2In$ or $CaC_2$ has not been previously obtained. In this regard, we should emphasize that the $Ni_2In$-type structure has not been tested for $TiO_2$, while $CaC_2$ has been proposed for $TiO_2$ [33,36]. Therefore, to our knowledge, we provide the EOS of the $Ni_2In$ and $CaC_2$ phases of $TiO_2$ for the first time (Table 1). When comparing the EOS for the three phases, we notice that $Fe_2P$ has the highest bulk modulus and thus is the most incompressible phase, followed by $CaC_2$ and finally $Ni_2In$ that exhibits the most compressibility among all tested phases. In detail, a small bulk modus decrease (~7%) is predicted across $Fe_2P \rightarrow CaC_2$, while we note an obviously large decrease (~39%) across $Fe_2P \rightarrow Ni_2In$ (Table 1). Furthermore, the density of $CaC_2$ at zero pressure is higher than that of $Fe_2P$, as expected, which is not the case for $Ni_2In$ where the density is less than that of $Fe_2P$ by ~9% (Figure 2). We should note that such predicted large changes in $K_0$ and $V_0$ across $Fe_2P \rightarrow Ni_2In$ are likely to be unexpected across transitions to higher-pressure phases, whereas the corresponding changes across $Fe_2P \rightarrow CaC_2$ are much more reasonable.

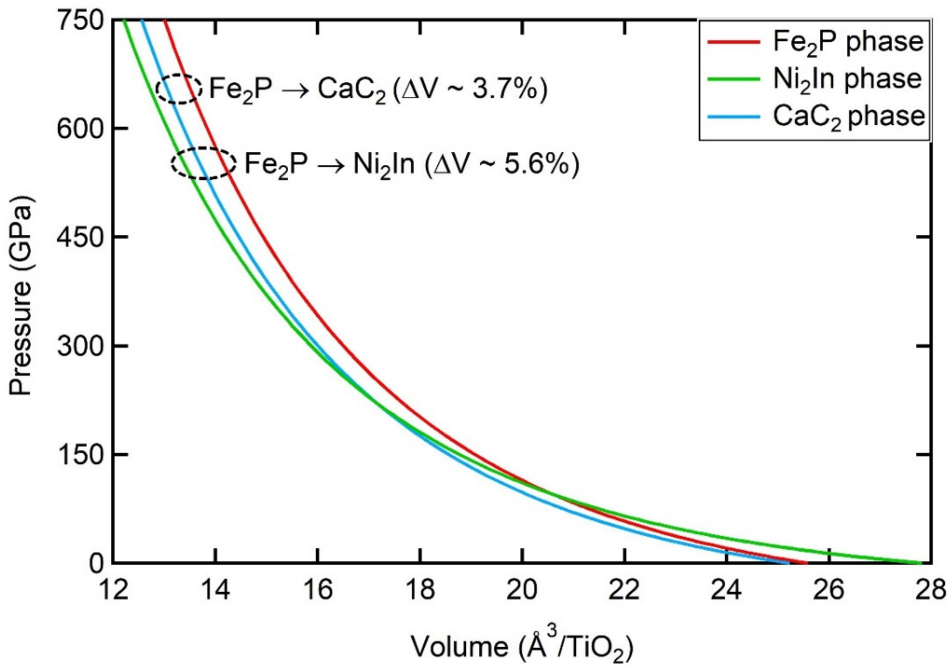


**Figure 2.** Pressure versus volume of $TiO_2$ phases as determined by GGA calculations using BM-EOS [57]. The dashed circles show the large volume reduction across the $Fe_2P \rightarrow Ni_2In$ and $Fe_2P \rightarrow CaC_2$ transitions.

To obtain the transition pressures, we calculated the enthalpy change relative to the $Fe_2P$ phase (Figure 3). First, we note that the transition from $Ni_2In$ to $CaC_2$ or vice versa is not possible at ultrahigh pressures as their enthalpy curves are unlikely to intersect. Furthermore, although the enthalpy curves of the two phases seem to cross at lower pressures, this transition is not expected to occur within the stability field of the $Fe_2P$ phase. Our enthalpy calculations indicate that the transition pressure across the $Fe_2P \rightarrow Ni_2In$ transition is 564 GPa. On the other hand, our calculated transition pressure across the $Fe_2P \rightarrow CaC_2$ transition is 664 GPa, in agreement with previous findings (Table 2) [33,36]. We should note that although the $Ni_2In$ phase has a lower enthalpy than the $CaC_2$ phase, this does not necessarily mean that $Fe_2P \rightarrow Ni_2In$ is the favorable transition when compared to the $Fe_2P \rightarrow CaC_2$ transition. Consequently, there are two possible scenarios for the transition from the $Fe_2P$ phase, and thus one must be eliminated from the transition sequence of $TiO_2$. Therefore, in the next sections, we further explore the two transitions to predict the favored post-$Fe_2P$ phase of $TiO_2$.

### *3.2. Enthalpy Difference and Volume Collapse across Phase Transitions*

In this section, we discuss the enthalpy difference across the two transitions and the contribution of the volume change in this difference as well as the correlation between the volume decrease and the coordination number increase. We note that the $Fe_2P \rightarrow Ni_2In$ and $Fe_2P \rightarrow CaC_2$ transitions are associated with a large enthalpy difference (Figure 3, Table 3) across the phase transition. Our calculations reveal that such noticeable enthalpy difference is mainly due to the obvious volume reduction across both transitions (Figure 2, Table 3), while the contribution of electronic energy gain has a minimal effect.

Although both transitions are driven by a large enthalpy change as discussed above, it has been found that the $Fe_2P \rightarrow Ni_2In$ transition requires a larger enthalpy change compared to the $Fe_2P \rightarrow CaC_2$ transition. This result is not unexpected and can be explained in view of the coordination number change across transitions; in this regard, we notice that the $Fe_2P \rightarrow Ni_2In$ is related to a 2-coordination-number increase (from 9 to 11) whereas $Fe_2P \rightarrow CaC_2$ is driven by a 1-coordination-number increase (from 9 to 10).

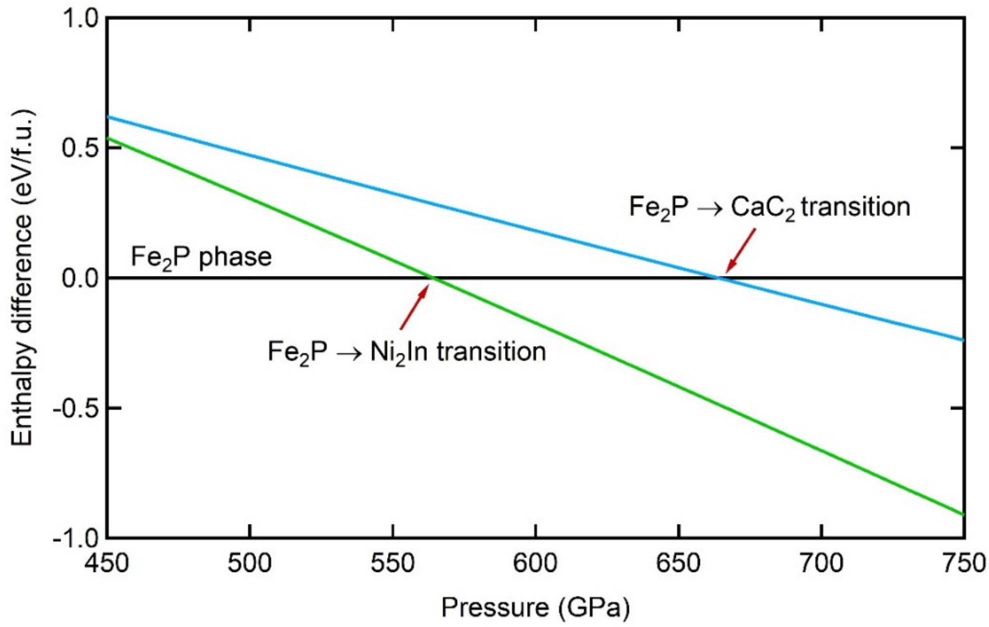


**Figure 3.** Change in enthalpy with respect to $Fe_2P$ phase versus pressure of one formula unit as determined by GGA calculations for $TiO_2$. The transition pressures across transitions from $Fe_2P$ to $Ni_2In$ and $CaC_2$ phases are shown.

**Table 2.** Calculated transition pressures across the $Fe_2P \rightarrow Ni_2In$ and $Fe_2P \rightarrow CaC_2$ phase transitions for $TiO_2$. For comparison, we list other calculated results.

| Phase Transition | Transition Pressure (GPa) | Reference |
|---|---|---|
| $Fe_2P \rightarrow Ni_2In$ | 564 GPa | This work |
| $Fe_2P \rightarrow CaC_2$ | 647 GPa<br>689 GPa<br>664 GPa | [36]<br>[33]<br>This work |

**Table 3.** Enthalpy difference, band gap difference, volume change, and coordination number change across the $Fe_2P \rightarrow Ni_2In$ and $Fe_2P \rightarrow CaC_2$ phase transitions for $TiO_2$.

| Phase Transition | $\Delta H/\Delta P$ | | Band Gap Difference (eV) | Volume Change (%) | Coordination Number Change |
|---|---|---|---|---|---|
| | eV·GPa$^{-1}$ ($\times 10^{-4}$) | kJ·mol$^{-1}$·GPa$^{-1}$ | | | |
| $Fe_2P \rightarrow Ni_2In$ | −48.102 | −0.46411 | 0.04 | 5.6 | 2 |
| $Fe_2P \rightarrow CaC_2$ | −28.135 | −0.27416 | 0 | 3.7 | 1 |

However, regardless of the coordination number increase (either 1 or 2), the calculated volume collapse across both transitions does not show a large difference (3.7% for $CaC_2$ vs. 5.6% for $Ni_2In$), where $Fe_2P \rightarrow Ni_2In$ is expected to show a much larger volume reduction due to the large coordination increase across this transition. In detail, it has been previously found that for $TiO_2$, the 2-coordination increase (from 7 to 9 in OI → OII transition) results in an ~ 8% volume reduction [29] compared to a 5.6% reduction for the same coordination increase in $Fe_2P \rightarrow Ni_2In$. On the other hand, the 3.7% volume decrease in $Fe_2P \rightarrow CaC_2$ transition looks more appropriate for a 1-coordination increase and agrees well with previous studies that reported values of 3.3–3.4% [33,36]. Therefore, based on the interplay between the volume reduction and coordination number change, the $Fe_2P \rightarrow CaC_2$ transition is likely favorable in $TiO_2$ when compared to the $Fe_2P \rightarrow Ni_2In$ transition.

### 3.3. Band Gap Calculations at the Transition Pressures

To further investigate the proposed ultrahigh-pressure phases of titania, we explored the pressure dependence of the band gap by analyzing the band structure of each phase at different pressures (Figures 4 and 5). Often, DFT calculations systematically underestimate band gaps; however, they accurately describe the pressure dependence [58,59]. We speculate that such analysis might be helpful in gaining a deeper insight into the $Fe_2P \rightarrow Ni_2In$ and $Fe_2P \rightarrow CaC_2$ transitions to better determine the favorable phase transition. Our band gap calculations show that the band gap of the $Fe_2P$-type structure at zero pressure is ~0.94 eV and decreases as pressure increases, where the drop in the band gap becomes more obvious at megabar pressures (Figure 4). However, regardless of such band-gap collapse, we should note that the $Fe_2P$ phase remains a semiconductor up to multi-megabar pressures before its metallization begins at pressures greater than 650 GPa (Figure 4), in good agreement with previous predictions obtained for $Fe_2P$-$TiO_2$ [33,36].

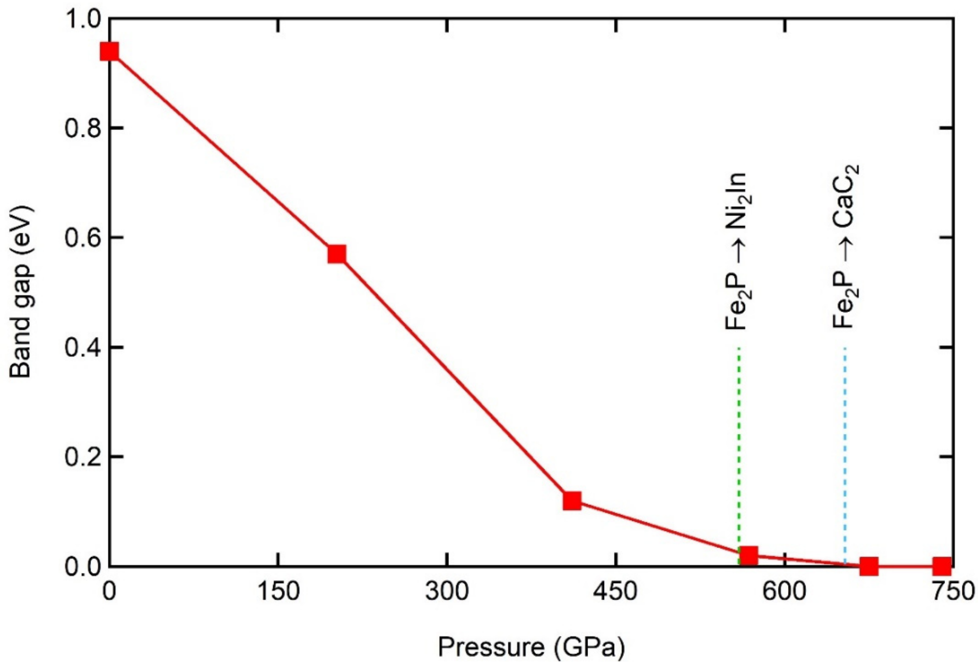


**Figure 4.** Calculated band gap of the $Fe_2P$ phase as a function of pressure. The vertical dashed lines indicate the transition pressures of the $Fe_2P \rightarrow Ni_2In$ and $Fe_2P \rightarrow CaC_2$ transitions.

Additionally, our analysis of the band structures of the $Ni_2In$ and $CaC_2$ phases reveals that both structures have metallic characteristics (band gap = 0 eV) at their predicted transition pressures from the $Fe_2P$ phase (Figures 4 and 5, Table 2). In this regard, we note that the band gap difference (Table 2, Figure 4) across $Fe_2P \rightarrow CaC_2$ transition is zero (0 eV $\rightarrow$ 0 eV) compared to a ~0.04 eV difference across $Fe_2P \rightarrow Ni_2In$ transition (0.04 eV $\rightarrow$ 0 eV). Consequently, our band gap calculations likely provide further evidence that supports the $Fe_2P \rightarrow CaC_2$ transition being the favorable transition when compared to the $Fe_2P \rightarrow CaC_2$ transition. Thus, we confirm previous theoretical findings that predict $CaC_2$ to be the post-$Fe_2P$ phase for $TiO_2$ [33,36]. Finally, it should be noted that such confirmation is important since the $Ni_2In$ phase was a highly possible scenario for $TiO_2$ as it has been predicted to be the post-$Fe_2P$ phase in the similar dioxides $ZrO_2$ and $HfO_2$ [42–44]. In this regard, we should emphasize that the three dioxides undergo the same transition sequence at high pressures (MI $\rightarrow$ OI $\rightarrow$ OII $\rightarrow$ $Fe_2P$), but the post-$Fe_2P$ phase in $TiO_2$ (i.e., $CaC_2$-type) is predicted to be different from that of $ZrO_2$ and $HfO_2$ (i.e., $Ni_2In$-type).

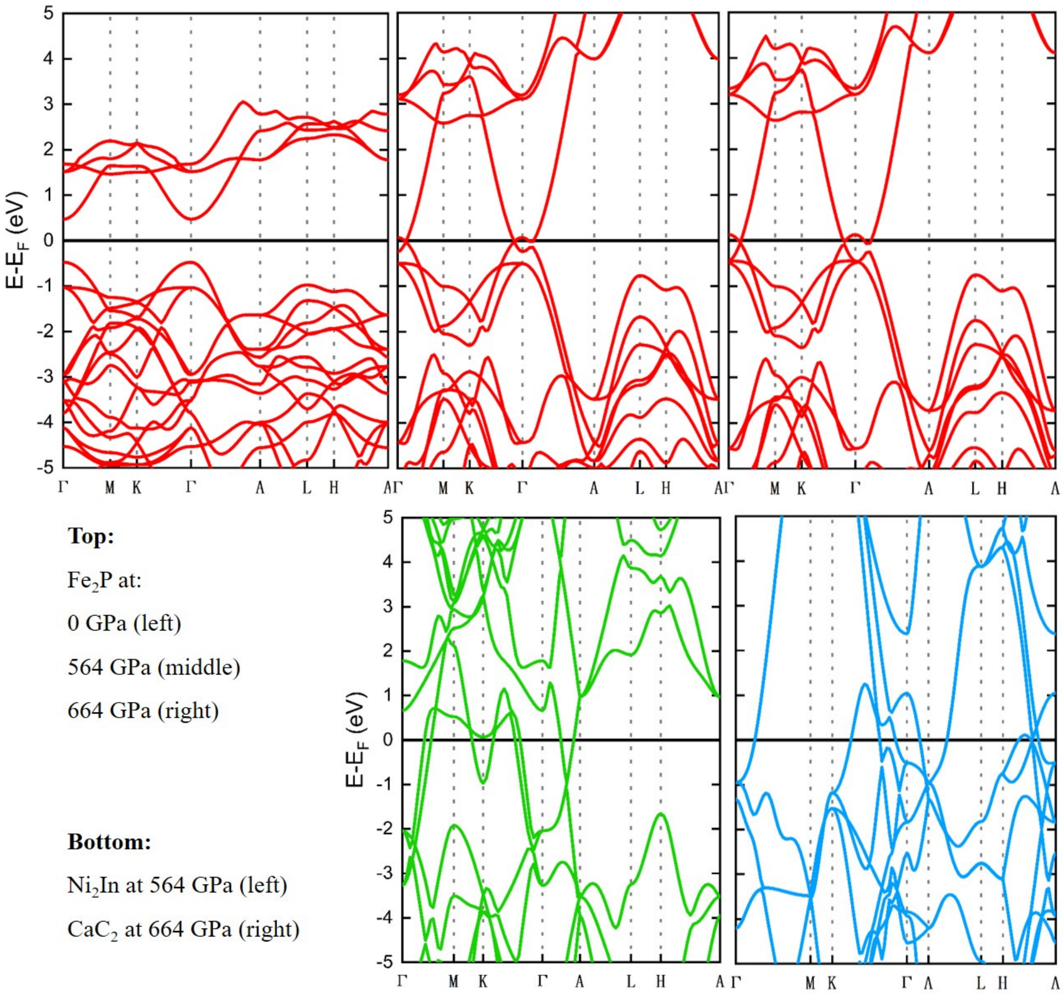


**Figure 5.** Electronic band structure for: (**Top**) the $Fe_2P$ phase at 0 GPa, 564 GPa, and 664 GPa; (**Bottom**) the $Ni_2In$ and $CaC_2$ phases at 564 GPa and 664 GPa, respectively.

## 4. Conclusions

In conclusion, we employed DFT computations to investigate the ultrahigh-pressure phase stability of the $Ni_2In$ and $CaC_2$ structures with respect to the $Fe_2P$ structure of titania. We explored the $Fe_2P \rightarrow Ni_2In$ and $Fe_2P \rightarrow CaC_2$ transitions to better predict the favored post-$Fe_2P$ of $TiO_2$. These transitions were thoroughly studied in terms of the volume decrease, the coordination number increase, and the band gap reduction. Our analysis favored the $Fe_2P \rightarrow CaC_2$ transition, and thus we predict that the $CaC_2$-type structure is likely the post-$Fe_2P$ phase of $TiO_2$, and therefore the most stable phase of titania at pressures that exceed 664 GPa. This result is also evidenced by a similar conclusion we recently obtained for $ZrO_2$, where the $Fe_2P \rightarrow CaC_2$ transition was predicted to be more favorable than the $Fe_2P \rightarrow Ni_2In$ transition (unpublished), thus emphasizing the close similarities of the high-pressure behavior of titania and zirconia. Finally, our equation of state determination shows that $CaC_2$ is the densest phase with a high bulk modulus that is comparable to that of the experimentally observed $Fe_2P$ phase, while the $Ni_2In$ phase reveals a low density and high compressibility.

**Author Contributions:** Conceptualization, Y.A.-K. and K.T.; methodology, Y.A.-K.; software, K.T.; formal analysis, Y.A.-K. and K.T.; writing—original draft preparation, K.T. and Y.A.-K.; writing—review and editing, Y.A.-K. and K.T. All authors have read and agreed to the published version of the manuscript.

**Funding:** This research received no external funding.

**Data Availability Statement:** The data presented in this study are available in the article.

**Conflicts of Interest:** The authors declare no conflict of interest.

## References

1. Wu, X. Applications of Titanium Dioxide Materials. In *Titanium Dioxide—Advances and Applications*; IntechOpen: London, UK, 2022.
2. Basheer, C. Application of Titanium Dioxide-Graphene Composite Material for Photocatalytic Degradation of Alkylphenols. *J. Chem.* **2013**, *2013*, 456586. [CrossRef]
3. Nishio-Hamane, D.; Shimizu, A.; Nakahira, R.; Niwa, K.; Sano-Furukawa, A.; Okada, T.; Yagi, T.; Kikegawa, T. The Stability and Equation of State for the Cotunnite Phase of $TiO_2$ up to 70 GPa. *Phys. Chem. Miner.* **2009**, *37*, 129–136. [CrossRef]
4. Swamy, V.; Kuznetsov, A.Y.; Dubrovinsky, L.S.; Kurnosov, A.; Prakapenka, V.B. Unusual Compression Behavior of Anatase $TiO_2$ Nanocrystals. *Phys. Rev. Lett.* **2009**, *103*, 75505. [CrossRef] [PubMed]
5. Shul'ga, Y.M.; Matyushenko, D.V.; Golyshev, A.A.; Shakhrai, D.V.; Molodets, A.M.; Kabachkov, E.N.; Kurkin, E.N.; Domashnev, I.A. Phase Transformations in Nanostructural Anatase $TiO_2$ under Shock Compression Conditions Studied by Raman Spectroscopy. *Tech. Phys. Lett.* **2010**, *36*, 841–843. [CrossRef]
6. Ding, Y.; Chen, M.; Wu, W. Mechanical Properties, Hardness and Electronic Structures of New Post-Cotunnite Phase ($Fe_2P$-Type) of $TiO_2$. *Phys. B Condens. Matter* **2014**, *433*, 48–54. [CrossRef]
7. Wang, Z.; Saxena, S.K. Raman Spectroscopic Study on Pressure-Induced Amorphization in Nanocrystalline Anatase ($TiO_2$). *Solid State Commun.* **2001**, *118*, 75–78. [CrossRef]
8. Gerward, L.; Olsen, J.S. Post-Rutile High-Pressure Phases in $TiO_2$. *J. Appl. Crystallogr.* **1997**, *30*, 259–264. [CrossRef]
9. Wang, Z.; Saxena, S.K.; Pischedda, V.; Liermann, H.P.; Zha, C.S. X-Ray Diffraction Study on Pressure-Induced Phase Transformations in Nanocrystalline Anatase/Rutile ($TiO_2$). *J. Phys. Condens. Matter* **2001**, *13*, 8317–8323. [CrossRef]
10. Swamy, V.; Dubrovinsky, L.S.; Dubrovinskaia, N.A.; Langenhorst, F.; Simionovici, A.S.; Drakopoulos, M.; Dmitriev, V.; Weber, H.-P. Size Effects on the Structure and Phase Transition Behavior of Baddeleyite $TiO_2$. *Solid State Commun.* **2005**, *134*, 541–546. [CrossRef]
11. Dubrovinskaia, N.A.; Dubrovinsky, L.S.; Ahuja, R.; Prokopenko, V.B.; Dmitriev, V.; Weber, H.-P.; Osorio-Guillen, J.M.; Johansson, B. Experimental and Theoritical Identification of a New High-Pressure $TiO_2$ Polymorph. *Phys. Rev. Lett.* **2001**, *87*, 275501. [CrossRef]
12. Caravaca, M.A.; Mino, J.C.; Perez, V.J.; Casali, R.A.; Ponce, C.A. Ab Initio Study of the Elastic Properties of Single and Polycrystal $TiO_2$, $ZrO_2$ and $HfO_2$ in the Cotunnite Structure. *J. Phys. Condens. Matter* **2009**, *21*, 15501. [CrossRef] [PubMed]
13. Hearne, G.R.; Zhao, J.; Dawe, A.M.; Pischedda, V.; Maaza, M.; Nieuwoudt, M.K.; Kibasomba, P.; Nemraoui, O.; Comins, J.D. Effect of Grain Size on Structural Transitions in Anatase $TiO_2$: A Raman Spectroscopy Study at High Pressure. *Phys. Rev. B* **2004**, *70*, 134102. [CrossRef]
14. Swamy, V.; Kuznetsov, A.; Dubrovinsky, L.S.; McMillan, P.F.; Prakapenka, V.B.; Shen, G.; Muddle, B.C. Size-Dependent Pressure-Induced Amorphization in Nanoscale $TiO_2$. *Phys. Rev. Lett.* **2006**, *96*, 135702. [CrossRef] [PubMed]
15. Ahuja, R.; Dubrovinsky, L.S. High-Pressure Structural Phase Transitions in $TiO_2$ and Synthesis of the Hardest Known Oxide. *J. Phys. Condens. Matter* **2002**, *14*, 10995–10999. [CrossRef]
16. Wang, Y.; Zhao, Y.; Zhang, J.; Xu, H.; Wang, L.; Luo, S.; Daemen, L.L. In Situ Phase Transition Study of Nano- and Coarse-Grained $TiO_2$ under High Pressure/Temperature Conditions. *J. Phys. Condens. Matter* **2008**, *20*, 125224. [CrossRef]
17. Flank, A.-M.; Lagarde, P.; Itie, J.-P.; Hearne, G.R. Pressure-Induced Amorphization and a Possible Polyamorphism Transition in Nanosized $TiO_2$: An x-Ray Absorption Spectroscopy Study. *Phys. Rev. B* **2008**, *77*, 224112. [CrossRef]
18. Arlt, T.; Bermejo, M.; Blanco, M.A.; Gerward, L.; Jiang, J.Z.; Olsen, J.S.; Recio, J.M. High-Pressure Polymorphs of Anatase $TiO_2$. *Phys. Rev. B* **2000**, *61*, 14414. [CrossRef]
19. Mattesini, M.; de Almeida, J.S.; Dubrovinsky, L.; Dubrovinskaia, N.; Johansson, B.; Ahuja, R. High-Pressure and High-Temperature Synthesis of the Cubic $TiO_2$ Polymorph. *Phys. Rev. B* **2004**, *70*, 212101. [CrossRef]
20. Swamy, V.; Muddle, B.C. Ultrastiff Cubic $TiO_2$ Identified via First-Principles Calculations. *Phys. Rev. Lett.* **2007**, *98*, 35502. [CrossRef]
21. Swamy, V.; Dubrovinskaia, N.A.; Dubrovinsky, L.S. Compressibility of Baddeleyite-Type $TiO_2$ from Static Compression to 40 GPa. *J. Alloys Compd.* **2002**, *340*, 46–48. [CrossRef]
22. Muscat, J.; Swamy, V.; Harrison, N.M. First-Principles Calculations of the Phase Stability of $TiO_2$. *Phys. Rev. B* **2002**, *65*, 224112. [CrossRef]
23. Lyakhov, A.O.; Oganov, A.R. Evolutionary Search for Superhard Materials: Methodology and Applications to Forms of Carbon and $TiO_2$. *Phys. Rev. B* **2011**, *84*, 92103. [CrossRef]

24. Al-Khatatbeh, Y.; Lee, K.K.M.; Kiefer, B. Compressibility of Nanocrystalline $TiO_2$ Anatase. *Phys. Chem. C* **2012**, *116*, 21635–21639. [CrossRef]
25. Swamy, V.; Dubrovinsky, L.S.; Dubrovinskaia, N.A.; Simionovici, A.S.; Drakopoulos, M.; Dmitriev, V.; Weber, H.-P. Compression Behavior of Nanocrystalline Anatase $TiO_2$. *Solid State Commun.* **2003**, *125*, 111–115. [CrossRef]
26. Al-Khatatbeh, Y.; Lee, K.K.M. From Superhard to Hard: A Review of Transition Metal Dioxides $TiO_2$, $ZrO_2$, and $HfO_2$ Hardness. *J. Superhard Mater.* **2014**, *36*, 231–245. [CrossRef]
27. Van Gestel, T.; Sebold, D.; Kruidhof, H.; Bouwmeester, H.J.M. $ZrO_2$ and $TiO_2$ Membranes for Nanofiltration and Pervaporation. Part 2. Development of $ZrO_2$ and $TiO_2$ Toplayers for Pervaporation. *J. Memb. Sci.* **2008**, *318*, 413–421. [CrossRef]
28. Swamy, V.; Muddle, B.C. Pressure-Induced Polyamorphic Transition in Nanoscale $TiO_2$. *J. Aust. Cer. Soc.* **2008**, *44*, 1–5.
29. Al-Khatatbeh, Y.; Lee, K.K.M.; Kiefer, B. High-Pressure Behavior of $TiO_2$ as Determined by Experiment and Theory. *Phys. Rev. B* **2009**, *79*, 134114. [CrossRef]
30. Meng, X.; Wang, L.; Liu, D.; Wen, X.; Zhu, Q.; Goddard, W.A.; An, Q. Discovery of $Fe_2P$-Type Ti(Zr/Hf)$2O_6$ Photocatalysts toward Water Splitting. *Chem. Mater.* **2016**, *28*, 1335–1342. [CrossRef]
31. Dekura, H.; Tsuchiya, T.; Kuwayama, Y.; Tsuchiya, J. Theoretical and Experimental Evidence for a New Post-Cotunnite Phase of Titanium Dioxide with Significant Optical Absorption. *Phys. Rev. Lett.* **2011**, *107*, 45701. [CrossRef]
32. Fu, Z.; Liang, Y.; Wang, S.; Zhong, Z. Structural Phase Transition and Mechanical Properties of $TiO_2$ under High Pressure. *Phys. Status Solidi Basic Res.* **2013**, *250*, 2206–2214. [CrossRef]
33. Zhong, X.; Wang, J.; Zhang, S.; Yang, G.; Wang, Y. Ten-Fold Coordinated Polymorph and Metallization of $TiO_2$ under High Pressure. *RSC Adv.* **2015**, *5*, 54253–54257. [CrossRef]
34. Liang, Y.; Zhang, B.; Zhao, J. Mechanical Properties and Structural Identifications of Cubic $TiO_2$. *Phys. Rev. B* **2008**, *77*, 94126. [CrossRef]
35. Swamy, V.; Kuznetsov, A.; Dubrovinsky, L.S.; Caruso, R.A.; Shchukin, D.G.; Muddle, B.C. Finite-Size and Pressure Effects on the Raman Spectrum of Nanocrystalline Anatase $TiO_2$. *Phys. Rev. B* **2005**, *71*, 184302. [CrossRef]
36. Lyle, M.J.; Pickard, C.J.; Needs, R.J. Prediction of 10-Fold Coordinated $TiO_2$ and $SiO_2$ Structures at Multimegabar Pressures. *Proc. Natl. Acad. Sci. USA* **2015**, *112*, 6898–6901. [CrossRef]
37. Luo, W.; Yang, S.F.; Wang, Z.C.; Ahuja, R.; Johansson, B.; Liu, J.; Zou, G.T. Structural Phase Transitions in Brookite-Type $TiO_2$ under High Pressure. *Solid State Commun.* **2005**, *133*, 49–53. [CrossRef]
38. Machon, D.; Daniel, M.; Pischedda, V.; Daniele, S.; Bouvier, P.; LeFloch, S. Pressure-Induced Polyamorphism in $TiO_2$ Nanoparticles. *Phys. Rev. B* **2010**, *82*, 140102. [CrossRef]
39. Wang, Y.; Zhang, J.; Zhao, Y. Strength Weakening by Nanocrystals in Ceramic Materials. *Nano Lett.* **2007**, *7*, 3196–3199. [CrossRef]
40. Baty, S.R.; Burakovsky, L.; Errandonea, D. Ab Initio Phase Diagram of Copper. *Crystals* **2021**, *11*, 537. [CrossRef]
41. Diaz-Anichtchenko, D.; Errandonea, D. Comparative Study of the Compressibility of $M_3V_2O_8$ (M = Cd, Zn, Mg, Ni) Orthovanadates. *Crystals* **2022**, *12*, 1544. [CrossRef]
42. Durandurdu, M. Novel High-Pressure Phase of $ZrO_2$: An Ab Initio Prediction. *J. Solid State Chem.* **2015**, *230*, 233–236. [CrossRef]
43. Al-Khatatbeh, Y.; Tarawneh, K.; Hamad, B. The Prediction of a New High-Pressure Phase of Hafnia Using First-Principles Computations. *IOP Conf. Ser. Mater. Sci. Eng.* **2018**, *305*, 012006. [CrossRef]
44. Al-Taani, H.; Tarawneh, K.; Al-Khatatbeh, Y.; Hamad, B. The High-Pressure Stability of $Ni_2In$-Type Structure of $ZrO_2$ with Respect to OII and $Fe_2P$-Type Phases: A First-Principles Study. *IOP Conf. Ser. Mater. Sci. Eng.* **2018**, *305*, 012016. [CrossRef]
45. Kokalj, A. Computer Graphics and Graphical User Interfaces as Tools in Simulations of Matter at the Atomic Scale. *Comput. Mater. Sci.* **2003**, *28*, 155–168. [CrossRef]
46. Al-Khatatbeh, Y.; Lee, K.K.M.; Kiefer, B. Phase Diagram up to 105 GPa and Mechanical Strength of $HfO_2$. *Phys. Rev. B* **2010**, *82*, 144106. [CrossRef]
47. Al-Khatatbeh, Y.; Lee, K.K.M.; Kiefer, B. Phase Relations and Hardness Trends of $ZrO_2$ Phases at High Pressure. *Phys. Rev. B* **2010**, *81*, 214102. [CrossRef]
48. Al-Khatatbeh, Y.; Tarawneh, K.; Al-Taani, H.; Lee, K.K.M. Theoretical and Experimental Evidence for a Post-Cotunnite Phase Transition in Hafnia at High Pressures. *J. Superhard Mater.* **2018**, *40*, 374–383. [CrossRef]
49. Nishio-Hamane, D.; Dekura, H.; Seto, Y.; Yagi, T. Theoretical and Experimental Evidence for the Post-Cotunnite Phase Transition in Zirconia at High Pressure. *Phys. Chem. Miner.* **2015**, *42*, 385–392. [CrossRef]
50. Dutta, R.; Kiefer, B.; Greenberg, E.; Prakapenka, V.B.; Duffy, T.S. Ultrahigh-Pressure Behavior of $AO_2$ (A = Sn, Pb, Hf) Compounds. *J. Phys. Chem. C* **2019**, *123*, 27735–27741. [CrossRef]
51. Hohenberg, P.; Kohn, W. Inhomogeneous Electron Gas. *Phys. Rev.* **1964**, *136*, B864–B871. [CrossRef]
52. Kresse, G.; Joubert, D. From Ultrasoft Pseudopotentials to the Projector Augmented-Wave Method. *Phys. Rev. B* **1999**, *59*, 1758–1775. [CrossRef]
53. Blochl, P.E. Projector Augmented-Wave Method. *Phys. Rev. B* **1994**, *50*, 17953. [CrossRef] [PubMed]
54. Perdew, J.P.; Burke, K.; Ernzerhof, M. Generalized Gradient Approximation Made Simple. *Phys. Rev. Lett.* **1996**, *77*, 3865–3868. [CrossRef]
55. Giannozzi, P.; Baroni, S.; Bonini, N.; Calandra, M.; Car, R.; Cavazzoni, C.; Ceresoli, D.; Chiarotti, G.L.; Cococcioni, M.; Dabo, I.; et al. QUANTUM ESPRESSO: A Modular and Open-Source Software Project for Quantum Simulations of Materials. *J. Phys. Condens. Matter* **2009**, *21*, 395502. [CrossRef] [PubMed]

56. Monkhorst, H.J.; Pack, J.D. Special Points for Brillouin-Zone Integrations. *Phys. Rev. B* **1976**, *13*, 5188–5192. [CrossRef]
57. Birch, F. Elasticity and Constitution of the Earth's Interior. *J. Geophys. Res.* **1952**, *57*, 227–234. [CrossRef]
58. Bandiello, E.; Errandonea, D.; Martinez-Garcia, D.; Santamaria-Perez, D.; Manjón, F.J. Effects of High Pressure on the Structural, Vibrational, and Electronic Properties of Monazite-Type PbCrO 4. *Phys. Rev. B* **2012**, *85*, 024108. [CrossRef]
59. Borlido, P.; Schmidt, J.; Huran, A.W.; Tran, F.; Marques, M.A.L.; Botti, S. Exchange-Correlation Functionals for Band Gaps of Solids: Benchmark, Reparametrization and Machine Learning. *npj Comput. Mater.* **2020**, *6*, 96. [CrossRef]